

Contemporary Deformation of the Fenwei faulted zone From Global Positioning System Data

Zhi Yu Gao¹, Wei Li¹, Hong Bin Cheng², and Hao Zhang³

¹Institute of Geology, China Earthquake Administration

²Second Monitoring and Application Center, China Earthquake Administration

³Earthquake Administration of Jiangsu Province

November 24, 2022

Abstract

The Fenwei faulted zone is a region with high level of seismic hazard. Different models are proposed for the formation of the Fenwei faulted zone, but none has given its specific kinematic mechanism. Using updated GPS data covering the eastern China, we discover that although the Ordos block, the North China Plain and the South China block are moving in the southeast direction, the relative motion between them is obviously different: there is basically no shear slips inside the Weihe graben, and the extension rate across it is significant; in addition, the Shanxi graben system has roughly equal extensional and right-lateral strike-slip components. We suggest that rapid southeastward motion of the rigid South China block and the North China Plain, with respect to the Ordos block, has imposed intensive tectonic extension on the Fenwei faulted zone forming the contemporary deformation.

1 **Contemporary Deformation of the Fenwei faulted zone From Global Positioning System Data**

2 **Wei Li^{1,2} Zhi-Yu Gao^{1,*} Hong-Bin Cheng² Hao Zhang³**

3 ¹Institute of Geology, China Earthquake Administration, Beijing, China.

4 ²Second Monitoring and Application Center, China Earthquake Administration, Xi'an, China

5 ³Earthquake Administration of Jiangsu Province, Nanjing, China

6 *To whom correspondence should be addressed. Email: gzy0801@163.com

7 **Key Points:**

- 8 • Fenwei faulted zone is a region with high-level of earthquake hazard
- 9 • Fenwei faulted zone is undergoing significant tectonic extension and right-lateral strike-slip
- 10 • Relative motion between blocks contributes to the formation of the Fenwei faulted zone and repeated large
- 11 earthquakes with short intervals

12 **Abstract**

13 The Fenwei faulted zone is a region with high level of seismic hazard. Different models are proposed for the

14 formation of the Fenwei faulted zone, but none has given its specific kinematic mechanism. Using updated GPS

15 data covering the eastern China, we discover that although the Ordos block, the North China Plain and the South

16 China block are moving in the southeast direction, the relative motion between them is obviously different: there is

17 basically no shear slips inside the Weihe graben, and the extension rate across it is significant; in addition, the

18 Shanxi graben system has roughly equal extensional and right-lateral strike-slip components. We suggest that rapid

19 southeastward motion of the rigid South China block and the North China Plain, with respect to the Ordos block,

20 has imposed intensive tectonic extension on the Fenwei faulted zone forming the contemporary deformation.

21 **1. Introduction**

22 The Fenwei faulted zone (FFZ, including the Weihe graben and the Shanxi graben system) has been the

23 political and cultural center in western China with a dense population and prosperous economy. However, the FFZ

24 is also famous for its high level of earthquake hazards. There have been 8 earthquakes of magnitude greater than 6

25 and 2 earthquakes of magnitude greater than 7 so far (Figure 1).

26 The Fenwei faulted zone, located at the position of intersection and superposition between three major blocks

27 (the Ordos block, the North China Plain (NCP) and the South China block), has been an intensively active basin in

28 the Cenozoic. The Fenwei faulted zone whose trend is NEE to NNE from S to N is characterized by transtensional

29 right-lateral shear faults to the east, and is bounded by left-lateral shear extensional faults to the south. Over the

30 past three decades, different models have been developed to describe the tectonic evolution of the graben systems

31 around the Ordos block (Molnar and Tapponnier, 1975; Tapponnier and Molnar, 1977; Tian et al., 1992; Northrup

32 et al., 1995; Yin, 2010; Liu et al., 2007). Some researchers considered that the tectonic deformation and evolution

33 of the Ordos area are the result of the far-field Indo-Asian collision (Molnar and Tapponnier, 1975; Tapponnier and

34 Molnar, 1977). Alternatively, Some interpreted the idea that North China crustal thinning and volcanic activity

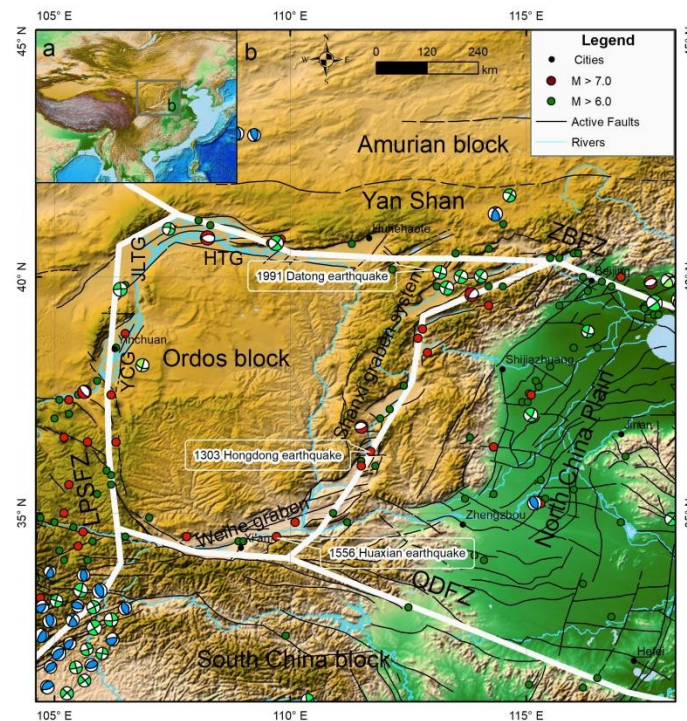
35 may be closely related to the westward subduction of the Pacific plate beneath the Eurasian continent and the

36 roll-back mechanism (Tian et al., 1992; Northrup et al., 1995).

37
38
39
40
41
42
43
44

45 Previous GPS observations from 1992 to 2002 show almost no deformation across the FFZ, neither extension
 46 nor strike slip (He et al., 2003; Shen et al., 2000; Wang et al., 2001). Zhang et al. (2018) used updated GPS data to
 47 conclude that there is no obvious east-west extension across either the Shanxi graben and the entire NCP. It is
 48 unlikely that a region with such frequent great historical earthquakes associated with no present-day deformation.
 49 There must be crustal deformation that has not yet been observed. Contradict the previous GPS studies, Modern
 50 seismicity indicates active rifting (Figure 1). Wesnousky et al. (1984) estimated a coseismic extension rate around
 51 ~1.0 mm/yr based on seismic moment data. This is close to the 0.5–1.6 mm/yr extension rate averaged over the
 52 Late Pliocene-Quaternary time (Zhang et al., 1998). Surface ruptures associated with great historical earthquakes
 53 on the graben-bounded faults do show prominent normal faulting with right-lateral strike-slip component such as
 54 the 1556 Huaxian earthquake (Rao et al., 2014), the 1303 Hongdong earthquake (Xu et al., 2014, 2019; Jiang et al.,
 55 2004). Fault plane solutions of recent earthquakes also show overwhelming dip-slip and strike-slip motions on
 56 almost vertical dipping NNE-trending faults planes such as the 1991 Datong earthquake (Figure 1; He et al., 2003;
 57 Xu et al., 2012, 2019; Chen & Nabelek, 1988; Gao et al., 2016). Hao et al. (2016) used precise leveling data
 58 observed in the period of 1970–2014 around the Ordos block to conclude that with respect to the stable Ordos, the
 59 Weihe and southern Shanxi grabens are subsiding at the rates of 4–6 mm/a. The subsidence of the Shanxi graben
 60 indicates that the graben is experiencing extensional movement on a long timescale.

61 Recently, Zheng et al. (2017) have published GPS velocity field that covers entire China and vicinity regions.
 62 In this paper we use a subset of their GPS data in the entire eastern China that spans three crustal blocks rather
 63 than restricting our analysis to only one block or one fault, trying to understand the pattern of contemporary
 64 tectonic deformation of the FFZ and earthquake hazards in the graben systems. The velocity field of tectonic
 65 deformation provides an important basis to understand the dynamic driving mechanism and is one of the keys to
 66 address the issues of Cenozoic deformation in eastern China.



67
 68 Figure 1. Seismotectonic map of the North China. (a) The thick gray lines outline boundaries of Figure 1b. (b) The bold white lines are
 69 block boundaries. Earthquake focal mechanism (>4.0) is taken from <http://www.ceic.ac.cn/>. HTG: Hetao graben; ZBFZ:
 70 Zhangjiakou-Bohai fault zone; QDFZ: Qinling-Dabie fault zone; LPSFZ: Liupanshan fault zone; YCG: Yinchuan graben; JLTG: Jilantai
 71 graben.

72 **2. Geological setting**

73 The Ordos block is characterized by low strain rate and seismicity. In contrast, the margins of this stable block
74 have been active since Cenozoic. The block is surrounded by four graben systems: the Yinchuan graben along its
75 western margin, the Hetao graben along its northern margin, the Shanxi graben system along its eastern margin,
76 and the Weihe graben along its southern margin (Yin et al., 2010; Zhao et al., 2017, Figure 1).

77 During the Yanshan movement, the Ordos block showed intermittent uplift and subsidence movements, while
78 strong tectonic activities occurred on its periphery. In the Hetao and Weihe basins, a near east-west trend
79 compressional tectonic belt is formed, while a NE-NNE trend compressional tectonic belt is formed in the Shanxi
80 and Yinchuan basins. The basic tectonic setting formed by the Mesozoic, especially the Yanshan movement, laid
81 the foundation for the geological evolution in this area in the Cenozoic. During the Cenozoic era, the most
82 outstanding features of the southwestern margin and adjacent areas of Ordos were the formation of a series of
83 extensional faulted basins on its periphery and the formation of thrusting fault zone on its southwestern margin.
84 According to the sediment distribution of the Ordos block and the developmental characteristics of the faulted
85 zones, the tectonic activities of the area can be roughly divided into three main stages: (1) the Weihe basin, the
86 Yinchuan basin and the Jilantai basin begin to develop in the Eocene. It had basically formed at the end of the
87 Oligocene. (2) at the end of the Miocene, the Ordos Block continued to uplift. and the peripheral faulted zones
88 continued to develop. In addition, the Weihe faulted zone extended eastward into Shanxi, forming the Yuncheng
89 basin; (3) at the end of the Pliocene, controlled by the NE-NNE trend faults, the Shanxi faulted zone was basically
90 formed. (Deng et al., 1999; Zheng et al., 2006; Wang et al., 2010; Wang et al., 2013; Chen et al., 2013; Shi et al.,
91 2013; Chen et al., 2015; Zhao et al., 2017; Working Group of the Active Fault Zone Around the Ordos, Chinese
92 Seismological Bureau, 1988).

93 The northern boundary of the Ordos block and NCP consists of the EW-trending Hetao graben and the
94 Zhangjiakou-Bohai fault zone (Figure 1), separating the North China block from Yan Shan mountains or the
95 Amurian block (Zhang et al., 2018; Figure 1). The southern boundary of the Ordos block and NCP is the
96 approximately EW-trending Qinling-Dabie Shan range-front fault zone (Figure 1). Geomorphological and
97 seismological studies suggest that this fault zone has limited Quaternary tectonic activity (Deng et al., 2003; Zhang,
98 Deng, et al., 2003).

99 The western boundary of the NCP is the Shanxi graben system where great historical earthquakes occurred
100 mostly inside the sedimentary basin, suggesting intensive tectonic activity on this boundary. The western boundary
101 of the Ordos block is the NS-trending Jilantai-Yinchuan graben and the Liupanshan thrust-fold zone, which both
102 have intensive tectonic activity and seismicity.

103
104
105
106
107
108
109
110
111
112
113
114
115

116 3. Pattern and Rate of Deformation From GPS Analyses

117 3.1. GPS Data and Relative Motion Among the Crust Blocks in Eastern China

118 The principal data used for this study come from the Crustal Movement Observation Network of China
119 collected during 1998 to 2015. The procedures of data collection and process are described recently in detail by
120 Zheng et al. (2017).

121 Figure 2 depicts motions of different crustal blocks relative to the fixed Eurasia. Stations in the Ordos block,
122 move with respect to the fixed Eurasia at velocities of 4 to 7 mm/yr in the directions ranging from N100° to 130°E
123 (Figure 2), suggesting almost a stable relative motion between the Ordos block and Eurasian plate.

124 Most of the GPS velocity vectors in the NCP are within the rates of 5.0 ± 1.5 mm/yr and the directions of
125 N100°–120°E (Figure 2) despite of isolated large local variations. It is worth to note that the velocities gradually
126 increase from 1–2 mm/yr in the Amurian block to 5–6 mm/yr in the interior of NCP (Figure 2, Zhang et al., 2018).

127 The South China block is regarded as a tectonically stable block due to the absence of active faults and strong
128 earthquakes (Deng et al., 2003; Zhang, Deng, et al., 2003). GPS velocities show coherent movement of the South
129 China with a rate of 7–8 mm/yr in the directions of N100°–120°E (Figure 2, Zhang et al., 2018). No velocity
130 gradient can be identified in the rigid South China block. Similar to the northern edge of NCP, the average 5–6
131 mm/yr relative motions near the southern edge of NCP gradually change to average 7–8 mm/yr velocities in the
132 South China block (Figure 2, Zhang et al., 2018).

133 3.2 Velocity Profiles in the Direction of N0°E

134 The N0°E velocity profiles is constructed to explore the movement differences between the South China
135 block and the Ordos block (the gray polygon in Figure 2). It can be seen from N90°E velocity components in the
136 direction of N0°E velocity profiles that there is a obvious left-lateral strike-slip rate difference of 2.27 ± 0.52
137 mm/yr between the South China block and the Ordos block within a distance of about 200km across the Weihe
138 graben (Fig 3a). Figure 3b shows that both the South China block and the Ordos block move southward at the rate
139 of -2.78 ± 0.98 mm/yr and -2.27 ± 0.80 mm/yr, respectively. The 0.51 ± 0.18 mm/yr rate difference demonstrates
140 that the extension rate of the Weihe graben in the NS direction is relatively small, but can be detected easily.

141 Wang et al. (2011) reported the predicted fault slip rates of the Weihe rift that the Weihe rift has a left-lateral
142 strike-slip rate of 1.4 ± 0.5 mm/yr and extension rate of 0.5 ± 0.3 mm/yr. These results are comparable with our
143 estimates.

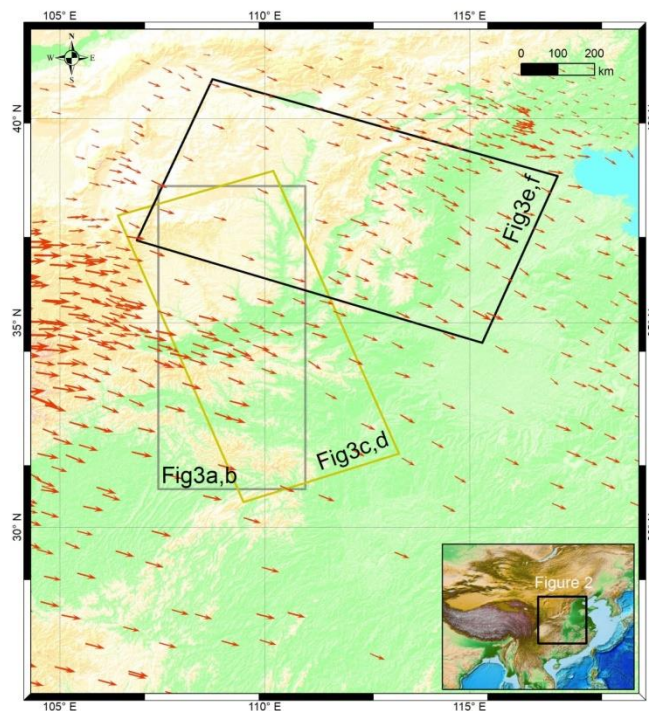
144
145
146
147
148
149
150
151
152
153
154
155
156
157
158
159

160 **3.3 Velocity Profiles in the Direction of N160°E**

161 We have constructed velocity profiles across the South China block and the Ordos block in the direction of
162 N160°E to study if there are differential motions perpendicular to the main structure trend in the Weihe graben (the
163 yellow polygon in Figure 2; Figure 3c and 3d).

164 From N70°E velocity components basically parallel to the main structural lines of the Weihe graben in the
165 N160°E velocity profiles (Figure 3c), we can find that there is no obvious differences in shear slip rates across the
166 Weihe graben indicating that the formation of the Weihe graben may not be related to the strike-slip movements
167 of the internal faults in the graben or the contemporary deformation of the Weihe graben is not dominated by
168 strike-slip movements.

169 In Figure 3d, although both the Ordos block and the South China block move southeastwards, however, there
170 are obvious rate differences on both sides of the Weihe graben or across the Husshan Fault. From the beginning to
171 a distance of ~ 400km, the rates remain within a stable range of ~ 4.0 mm/yr. But the rates show an rapid growth
172 while entering the South China block. The rates maintains averaged ~ 5 mm/yr in the interior of the South China
173 block (Figure 3d). The rate difference of about ~ 1 mm/yr between the South China block and the Ordos block in
174 the N160°E direction, which is twice as much the extension rate in the direction of N0°E velocity profiles means
175 that the main extensional direction of the Weihe graben is NW-SE trend. The seismogenic fault of the catastrophic
176 1556 Huaxian earthquake killing 800 thousands people is thought to be the roughly NE-NEE trend Huashan fault.
177 The fault is a Holocene active fault, controlling the Quaternary subsidence center of the Weihe basin and the
178 highest terrain. Interestingly, the ~ 1mm/yr we observed is basically equivalent to the ~ 1mm/yr dip-slip rate of the
179 Huashan fault from geologic studies (Xu et al.,2017; Yang et al., 2012; Li et al., 2015; Li et al., 1983; Rao et al.,
180 2014) indicating the Huashan fault absorbs the main extension deformation.



181
182 Figure 2. Global Positioning System (GPS) velocity field of the North China in the Eurasia fixed reference frame. The gray polygon
183 marks data used to plot Figures 3a and 3b. The yellow polygon covers velocity vectors plotted in Figures 3c and 3d. The black polygon
184 covers velocity vectors plotted in Figures 3e and 3f. The insert shows the location of the figure. The GPS data are from Zheng et al.
185 (2017).
186

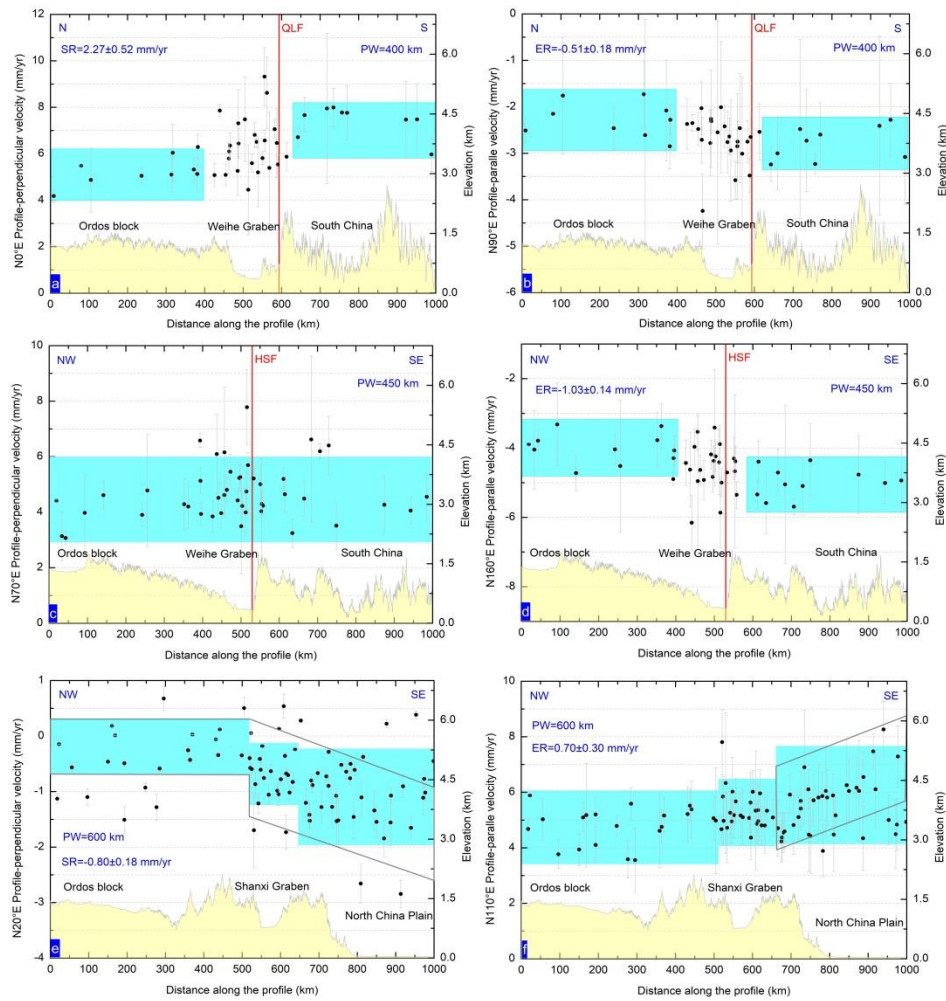
187 **3.4 Velocity Profiles in the Direction of N110°E**

188 To probe deformation of the Shanxi graben system we construct velocity profiles in the direction of N20°E
189 and plot velocity components of both N20°E and N110°E for stations in the Ordos block, the NCP (the black
190 polygon in Figure 2; Figures 3e and 3f).

191 The N20°E components of GPS stations plotted on the profile are intended to detect if there is strike-slip
192 movements between the Ordos block and the NCP in roughly NS orientation (Figure 3e). The profile obviously
193 depicts that both the Ordos block and NCP move slightly southward (Figure 3e). However, the profile across the
194 Shanxi graben system and NCP shows different kinematic patterns from the Ordos block (Figure 3e). Two
195 interpretations can be proposed. One is that rate differences across the Shanxi graben system behaves as step-wise
196 variety showing by the cyan rectangle in Figure 3e to result in about 0.8 mm/yr right-lateral strike-slip. The other
197 one, shown by the gray polygon, is that the rates increases progressively southeastward to create right-lateral
198 strike-slip within a broader range, whereas the Ordos block maintains its velocities within a stable range (Figure
199 3e).

200 The N110°E components of GPS stations plotted on the profile are intended to detect if there is extension or
201 contraction between the Ordos block and NCP in roughly EW orientation (Figure 3f). The profile obviously
202 depicts that both the Ordos block and NCP move eastward (Figure 3f). However, the profile across the Shanxi
203 graben system and NCP also shows different kinematic patterns from the Ordos block (Figure 3f). Two
204 interpretations can be proposed. One is that rate differences across the Shanxi graben system behaves as step-wise
205 variety showing by the cyan rectangle in Figure 3f to result in about 0.7 mm/yr extension rate. The other one,
206 shown by the gray polygon, is that the rates increases progressively southeastward within the NCP, whereas the
207 Ordos block maintains its velocities within a stable range (Figure 3f).

208 Wang et al. (2011) reported the predicted fault slip rates of the Shanxi rift that the Shanxi rift has a
209 right-lateral strike-slip rate of 0.6 ± 0.5 mm/yr and extension rate of 0.8 ± 0.3 mm/yr. These results are basically
210 consistent with our estimates.



211

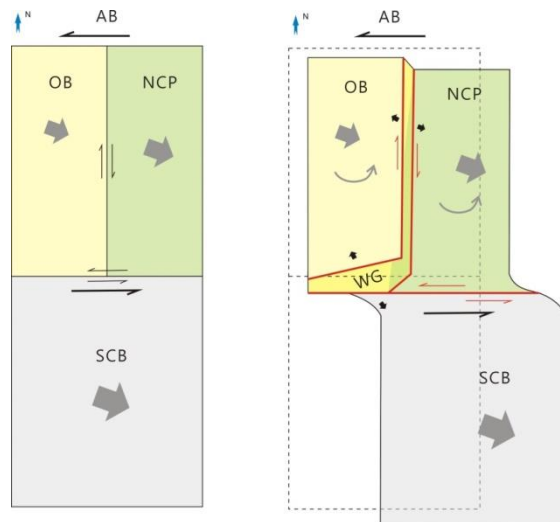
212 Figure 3. Global Positioning System (GPS) velocity profiles and swath profiles. GPS velocity components are designated that eastward
 213 and northward are positive. The cyan strips mark acceptable ranges of average velocity components. SR: strike-slip rate; ER: extension
 214 rate. PW: profile width. QLF: Qinling fault; HSF: Huashan fault. The locations of each profile are referred in Fig 2.

215 **4. Model of Deformation and seismicity**

216 The pattern of deformation of the FFZ is very different from the NCP (Zhang et al., 2018) where the roughly
 217 EW-trending left-lateral shear zone has been accommodated by a group of nearly NS-trending right-lateral faults
 218 and from the eastern Tibet (England & Molnar, 1990) where the NS-trending right-lateral shear zone bounds a
 219 group of EW-trending left-lateral faults within the zone (e.g., Zhang et al., 2018; England & Molnar, 1990; Nur et
 220 al., 1989; Savage et al., 2004).

221 Figure 4a shows original cartoon that the Ordos block and NCP behaves as a whole block and the South
 222 China block is rigid.

223 During the period of relative motion between different blocks, the South China block moves ESE-ward more
 224 rapidly than the Ordos block to create a left-lateral simple shear on the southern border of the Weihe graben and a
 225 extension to the Weihe graben in the both NS and SES direction (Figure 3, Figure 4b). The left-lateral simple shear
 226 provides space for the further expansion of the Weihe graben (Figure 4b). As the extension continuing, the pure
 227 shear might have taken advantage of weak zones forming a series of NEE-trending normal faults in the Weihe
 228 graben. The NEE-trending faults absorb most interseismic shearing to accumulate elastic strain. When strain
 229 accumulation exceeds the frictional strength of a particular NEE-trending fault, great earthquake occurs to release
 230 the accumulated strain. The earthquake rupture and permanent deformation are expected to be pure dip-slip on the
 231 NEE-trending faults (Figure 4b).



232

233 Figure 4. Conceptual cartoon diagram showing deformation pattern of the Weihe-Shanxi graben . (a) Original cartoon before deformation.
 234 (b) Pattern of permanent deformation in the long term induced by relative motion among the Weihe graben, the NCP and the South
 235 China block. The red lines shows active faults. The gray bold arrow denote direction and rate of the block motion. The small black bold
 236 arrow denote direction of the tectonic extension. AB: Amurian block; OB: Ordos block; NCP: North China Plain; SCB: South China
 237 block. WG: Weihe graben.

238 The NCP moves ESE-ward more rapidly than the Ordos block to create a right-lateral simple shear on the
 239 eastern border of the Ordos block and a extension to the Shanxi graben system in the ~ EW direction forming the
 240 Shanxi graben system (Figure 4b). The right-lateral strike-slip and extension rates are about 0.8 mm/yr and 0.7
 241 mm/yr respectively. This pattern of transextensional deformation contributes to the formation of a series of small
 242 pull-apart basins such as Linfen basin, Taiyuan basin and Datong basin from south to north. Geological and
 243 seismological observations support the scenario of this kind of deformation. Almost all great historical earthquakes
 244 in the Shanxi graben system occurred along the NNE-trending faults with both dip-slip displacements or strike-slip
 245 displacements. The surface ruptures of the 1303 Hongdong earthquake, for example, dominated by dip-slip
 246 displacements with some horizontal displacements from geological observations and paleoearthquake trenches (Xu
 247 et al., 2014, 2019; Jiang et al., 2004). The Hongdong M8.0 earthquake in 1303 was the earliest magnitude 8
 248 earthquake in China based on historical documents and the largest earthquake recorded in the Shanxi graben
 249 system. Fault plane solutions of large historical earthquakes (Figure 1) also manifest prominent right-lateral
 250 strike-slip displacements in the northern segment and dip-slip displacements in the southern segment (He et al.,
 251 2003).

252 This pattern of deformation of the FFZ causes repeated occurrences of large earthquakes with relatively short
 253 interseismic intervals (Xu et al., 2014, 2019). The characteristics of the FFZ could be summarized as follows: First,
 254 the strain produced by extension-induced pure shear can be easily concentrated on the main boundary faults.
 255 Second, due to continuing extension in the long run, the strain rate across each fault can be sustained to account for
 256 big earthquakes. Third, the secondary faults will be produced by earthquakes and accommodate the interseismic
 257 strain, which in turn could generate earthquakes.

258

259

260

261

262

263

264 **5. Discussion and Implication**

265 To summarize, the most important discovery of our new analysis of GPS data is that the contemporary
266 deformation of the FFZ is dominated by almost pure normal slip which is driven by the relative motion between
267 the Ordos block, NCP and the South China block (Figure 4). The extension is accommodated by right-lateral
268 strike-slips along the NNE-trending faults in the Shanxi graben system and left-lateral strike-slips between the
269 Ordos block and the South China block. This pattern of deformation provides important implications for
270 earthquake occurrences and geodynamics for the FFZ.

271 Seismic hazards and risks in the eastern section of the Weihe graben are much higher than its western section.
272 An important reason for this is that extension rates in the SES direction across the eastern section are ~2 times
273 bigger than the rates in the NS direction across the western section. While seismic hazards and risks in the Shanxi
274 graben system are also high. The reason for this is that the strike-slip and extension rates in the Shanxi graben
275 system are basically equivalent to each other. It is likely that future large earthquakes will continue to occur in the
276 whole Shanxi graben system on the NNE-trending faults with both dip-slips and right-lateral strike-slips.

277 The formation of the FFZ, as a Cenozoic extensional basin, was due to crustal extension and lithospheric
278 thinning associated with geological processes of “block motion”. Our results indicate that the processes that
279 driving the extension are continuing in a long time scale. The geodynamic processes that caused the processes are
280 unclear, but based on the maximum extension direction of the Weihe graben, we propose a combined model that
281 rapid eastward motion of the eastern China, driven by eastward growth of the Tibetan Plateau, has created the
282 eastward motion of the NCP and the South China block relative to the stable Ordos block, accompanied by the
283 westward subduction of the Pacific plate, accelerating the tectonic extension of the FFZ.

284 **Acknowledgments**

285 We thank all the GPS field crews for collecting the high-quality data that we used for this paper. We are
286 grateful to all the people who contribute to CMONOC-I/II. We also thank Zheng et al. (2017) for making the data
287 available for this study. This work was funded by National Natural Science Foundation of China (No.41631073).

288
289
290
291
292
293
294
295
296
297
298
299
300
301
302
303
304
305
306
307

308
309
310
311
312
313
314
315
316
317
318
319
320
321
322
323
324
325
326
327
328
329
330
331
332
333
334
335
336
337
338
339
340
341
342
343
344
345
346
347
348
349
350
351

References

- Chen, W. P., J. Nabelek (1988). Seismogenic strike-slip faulting and the development of the North China Basin. *Tectonics*, 7(5), 975–989.
<https://doi.org/10.1029/TC007i005p00975>
- Chen, Z., Burchfiel, B.C., Liu, Y., King, R.W., Royden, L.H., Tang, W., Wang, E., Zhao, J., Zhang, X. (2000). Global Positioning System measurements from eastern Tibet and their implications for India/Eurasia. *J. Geophys. Res.*, 105, 215–227.
<https://doi.org/10.1029/2000jb900092>
- Cheng, Y., He, C., Rao, G., Y, B., Lin, A., Hu, J., Yu, Y., Yao, Q. (2018). Geomorphological and structural characterization of the southern Weihe Graben, central China: Implications for fault segmentation. *Tectonophysics*, 722, 11–24.
- Deng, Q., Liao, Y. (1996). Paleoseismology along the range-front fault of Helan Mountains, north central China. *J. Geophys. Res.*, 101, 5873–5893.22.
- Deng, Q., Zhang, P., Ran, Y., Yang, X., Min, W., & Chu, Q. (2003). Basic characteristics of active tectonics of China. *Science in China Series D: Earth Sciences*, 46(4), 356–372.
- England, P., Molnar, P. (1990). Right-lateral shear and rotation as the explanation for strike-slip faulting in eastern Tibet. *Nature*, 344(6262), 140–142. <https://doi.org/10.1038/344140a0>
- Gan, W., Zhang, P., Shen, Z.K., Niu, Z., Wang, M., Wan, Y., Zhou, D., Cheng, J. (2007). Present-day crustal motion within the Tibetan Plateau inferred from GPS measurements. *J. Geophys. Res.*, 112, 1–14. <http://dx.doi.org/10.1029/2005JB004120>
- Gao, B., Jia, K., & Zhou, S. Y. (2016). Research of locations and source parameters of historical earthquakes equal and greater than m 5.0 from 1900 to 1970 in North China. *Chinese Journal of Geophysics*, 59(11), 4089–4099 (in Chinese with an English abstract).
- Hao, M., Wang, Q., Shen, Z., Cui, D., Ji, L., Li, Y., Qin, S. (2014). Tectonophysics Present day crustal vertical movement inferred from precise leveling data in eastern margin of Tibetan Plateau. *Tectonophysics* 632, 281–292.
<http://dx.doi.org/10.1016/j.tecto.2014.06.016>
- He, J., Liu, M., & Li, Y. (2003). Is the Shanxi rift of northern China extending? *Geophysical Research Letters*, 30(23), 2213.
<https://doi.org/10.1029/2003GL018764>
- Jiang, W., Deng, Q., Xu, X., Xie, X. (2004). Surface rupture zone of the 1303 Hongtong m = 8 earthquake, Shanxi province. *ACTA Seismol. Sin.*, 26, 355–362. <https://doi.org/10.1007/s11589-004-0018-0>
- Li D., Du J., Ma Y. (2015). Active faults and dip slip rates along the northern margins of the Huashan Mountain and Weinan loess tableland in the southeastern Weihe Graben, central China. *Journal of Asian Earth Sciences*, 114: 266–278.
- Li X., Ran Y. (1983). Active faults in the north slope of Huashan Mountain and the front of the Weinan tableland. *North China Earthquake Sciences*, 1(2): 10–18, 9 (in Chinese).
- Liu, G. (1987). The Cenozoic rift system of the North China Plain and the deep internal process. *Tectonophysics*, 133(3–4), 277–285.
[https://doi.org/10.1016/0040-1951\(87\)90270-8](https://doi.org/10.1016/0040-1951(87)90270-8)
- Liu, M., Shen, Z., Wang, S., Wang, M., Wang, Y. (2007). Active tectonics and intracontinental earthquakes in China: the kinematics and geodynamics. *Geol. Soc. Ame.*, 2425, 299–318. [http://dx.doi.org/10.1130/2007.2425\(19\)](http://dx.doi.org/10.1130/2007.2425(19))
- Ma, X.Y. (1987). Lithospheric Dynamics Map of China and Adjacent Seas (1:4,000,000) and Explanatory Notes. *Geological Publishing House*, China.
- Ma, Z., Chen, X., Ye, S., Nai, X., Wei, Z., Chen, J., Ning, J., Xu, H., Ding, G. (2001). Contemporary crustal movement of continental china obtained by global positioning system (GPS) measurements (in Chinese). *Sci. Bull.*, 46, 1118–1120.
- Meade, B.J. (2007). Algorithms for the calculation of exact displacements, strains, and stresses for triangular dislocation elements in a uniform elastic half space. *Comp. Geosci.*, 33, 1064–1075. <http://dx.doi.org/10.1016/j.cageo.2006.12.003>
- Min, W., Jiao, D., Chai, C., Zhang, P., Mao, F. (2003). Characteristics of the active Luoshan Fault since Late Pleistocene. North Central China. *Ann. Geophys*, 46.
- Molnar, P., Tapponnier, P. (1975). Cenozoic tectonics of Asia: effects of a continental collision. *Science*, 189, 419–426.
<http://dx.doi.org/10.1126/science.189.4201.419>
- Menzies, M. A., & Xu, Y. (1988). Geodynamics of the North China craton. In M. F. J. Flower, S. L. Chung, C. H. Lo, & T. Y. Lee (Eds.),

352 Mantle dynamics and plate interactions in East Asia (Vol. 27, pp. 155–165). Washington, DC: American Geophysical Union.

353 Niu, Z., Wang, M., Sun, H., You, X., Gan, W., Xue, G., Hao, J., Xin, S., Wang, Y., Wang, Q., Wang, Y.X., Li, B. (2005). Contemporary
354 velocity field of crustal movement of Chinese mainland from global positioning system measurements. *Chin. Sci. Bull.*, 50, 939–941.

355 Northrup, C.J., Royden, L.H., Burchfiel, B.C. (1995). Motion of the Pacific plate relative to Eurasia and its potential relation to Cenozoic
356 extension along the eastern margin of Eurasia. *Geology*, 23, 719–722. [http://dx.doi.org/10.1130/0091-7613\(1995\)](http://dx.doi.org/10.1130/0091-7613(1995)023<0719:MOTPPR>2.3.CO;2)
357 [023<0719:MOTPPR>2.3.CO;2](http://dx.doi.org/10.1130/0091-7613(1995)023<0719:MOTPPR>2.3.CO;2)

358 Nur, A., Ron, H., & Scotti, O. (1989). Kinematics and mechanics of tectonic block rotations. In S. C. Cohen & P. Vanicek (Eds.), *Slow*
359 *deformation and transmission of stress in the Earth*, Geophysical Monograph Series (Vol. 49, pp. 31–46). Washington, DC:
360 American Geophysical Union.

361 Rao, G., Lin, A., Yan, B., Jia, D., Wu, X. (2014). Tectonic activity and structural features of active intracratonic normal faults in the
362 Weihe Graben, central China. *Tectonophysics*, 638, 270–285.

363 Savage, J. C. (2000). Viscoelastic-coupling model for the earthquake cycle driven from below. *J. Geophys. Res.*, 105(B11), 25525–25532.
364 <https://doi.org/10.1029/2000JB900276>

365 Shen, Z.K., Lu, J., Wang, M., Bürgmann, R. (2005). Contemporary crustal deformation around the southeast borderland of the Tibetan
366 Plateau. *J. Geophys. Res.*, 110. <http://dx.doi.org/10.1029/2004JB003421>

367 Shen, Z. K., Wan, Y., Gan, W., Li, T., & Zeng, Y. (2004). Crustal stress evolution of the last 700 years in North China and earthquake
368 sequence (in Chinese with an English abstract). *Earthquake Research in China*, 20, 211–228.

369 Shen, Z.-K., Zhao, C., Zhao, A., Yin, Y., Li, D. D. J., Fang, P., & Dong, D. (2000). Contemporary crustal deformation in East Asia
370 constrained by global positioning system measurements. *J. Geophys. Res.*, 105(B3), 5721–5734.
371 <https://doi.org/10.1029/1999JB900391>

372 Tapponnier, P., Molnar, P. (1977). Active faulting and tectonics in China. *J. Geophys. Res.*, 82, 2905–2930.

373 Thatcher, W. (2007). Microplate model for the present-day deformation of Tibet. *J. Geophys. Res.*, 112, B01401.
374 <http://dx.doi.org/10.1029/2005JB004244>

375 Tian, Z., Han, P., Xu, K. (1992). The Mesozoic-Cenozoic East China rift system. *Tectonophysics*, 208, 341–363.
376 [http://dx.doi.org/10.1016/0040-1951\(92\)90354-9](http://dx.doi.org/10.1016/0040-1951(92)90354-9)

377 Wang, H., Liu, M., Cao, J., Shen, X., Zhang, G. (2011). Slip rates and seismic moment deficits on major active faults in mainland China.
378 *J. Geophys. Res.*, 116. <http://dx.doi.org/10.1029/2010JB007821>

379 Wang, M., Shen, Z.K., Niu, Z., Zhang, Z., Sun, H. (2003). Contemporary crustal deformation and active blocks model of China mainland
380 (in Chinese). *Sci. China, Ser.: D*, 33 (suppl.), 21–32.

381 Wang, Q., Zhang, P.-Z., Freymueller, J. T., Bilham, R., Larson, K. M., Xi'an, L., et al. (2001). Present-day crustal deformation in
382 continental China constrained by Global Positioning System measurements. *Science*, 294(5542), 574–577,
383 <https://doi.org/10.1126/science.1063647>

384 Wesnousky, S. G., L. M. Jones, C. H. Scholz, and Q. Deng (1984). Historical seismicity and rates of crustal deformation along the
385 margins of The Ordos block, North China. *Bull. Seism. Soc. Am.*, 74, 1767–1783.

386 Xu, W., Yang, Y., Yuan, Z. (2017). Late Quaternary faulted landforms and fault activity of the Huashan piedmont fault. *Geology and*
387 *Seismology*, 39(3), 587–604.

388 Xu, X., Ma, X., & Deng, Q. (1993). Neotectonic activity along the Shanxi rift system, China. *Tectonophysics*, 219(4), 305–325,
389 [https://doi.org/10.1016/0040-1951\(93\)90180-R](https://doi.org/10.1016/0040-1951(93)90180-R).

390 Xu Y. (2014). A study on the late Quaternary faulting of the Huoshan piedmont fault zone in the central Shanxi faulted basin belt. *Recent*
391 *Developments in World Seismology*, 6: 37–39.

392 Xu Y., He H., Deng Q., Allen M.B., Sun H., & Bi L. (2018). The CE 1303 Hongdong earthquake and the Huoshan Piedmont Fault,
393 Shanxi Graben: Implications for magnitude limits of normal fault earthquakes. *J. Geophys. Res.*, 123.
394 <https://doi.org/10.1002/2017JB014928>

395 Yang Y., Gao Z., Xu, W. (2012). Geomorphic expression and response of the activity along the middle section of Huashan front fault in

396 the late Quaternary period. *Technology for Earthquake Disaster Prevention*, 7(4): 335–347(in Chinese).

397 Yin, A. (2010). Cenozoic tectonic evolution of Asia: a preliminary synthesis. *Tectonophysics*, 488, 293–325,

398 <http://dx.doi.org/10.1016/j.tecto.2009.06.002>

399 Zhai, M. G. (2011). Cratonization and the ancient North China continent: A summary and review. *Science China Earth Sciences*, 54(8),

400 1110–1120. <https://doi.org/10.1007/s11430-011-4250-x>

401 Zhang, P.-Z., Deng, Q., Zhang, G., Ma, J., Gan, W., Min, W., et al. (2003). Active tectonic blocks and strong earthquakes in continental

402 China. *Science in China (Series D)*, 46, 13–24.

403 Zhang, Y., Ma, Y., Yang, N., Shi, W., & Dong, S. (2003). Cenozoic extensional stress evolution in North China. *Journal of Geodynamics*,

404 36, 591–613. <https://doi.org/10.1016/j.jog.2003.08.001>

405 Zhang, Y.Q., Mercier, J.L., Vergly, P. (1998). Extension in the graben systems around the Ordos (China), and its contribution to the

406 extrusion tectonics of south China with respect to Gobi-Mongolia. *Tectonophysics*, 285, 41–75.

407 [http://dx.doi.org/10.1016/S0040-1951\(97\)00170-4](http://dx.doi.org/10.1016/S0040-1951(97)00170-4)

408 Zhao, B., Zhang, C., Wang, D., Huang, Y., Tan, K., Du, R., Liu, J. (2017). Contemporary kinematics of the Ordos block, North China and

409 its adjacent rift systems constrained by dense GPS observations. *Journal of Asian Earth Sciences*, 135, 257–267.

410 <http://dx.doi.org/10.1016/j.jseas.2016.12.045>

411 Zheng, G., Wang, H., Wright, T. J., Lou, Y., Zhang, R., Zhang, W., & Wei, N. (2017). Crustal deformation in the India-Eurasia collision

412 zone from 25 years of GPS measurements. *J. Geophys. Res.*, 122, 9290–9312. <https://doi.org/10.1002/2017JB014465>

413 Zhu, R. X., Chen, L., Wu, F. Y., & Liu, J. L. (2011). Timing, scale and mechanism of the destruction of the North China craton. *Science*

414 *China Earth Sciences*, 54(6), 789–797. <https://doi.org/10.1007/s11430-011-4203-4>

415 Zhu, R. X., Xu, Y. G., Zhu, G., Zhang, H. F., Xia, Q. K., & Zheng, T. Y. (2012). Destruction of the North China craton. *Science China*

416 *Earth Sciences*, 55, 1565–1587. <https://doi.org/10.1007/s11430-012-4516-y>